© 2014. Published by The Company of Biologists Ltd | The Journal of Experimental Biology (2014) 217, 1925-1932 doi:10.1242/jeb.096248

RESEARCH ARTICLE

Convergence in morphology and masticatory function between the pharyngeal jaws of grass carp, *Ctenopharyngodon idella*, and oral jaws of amniote herbivores

Nicholas J. Gidmark*,‡, James C. Tarrant* and Elizabeth L. Brainerd

ABSTRACT

The cellulose-rich walls that protect plant cells are difficult to digest, and therefore mechanical food processing is a key aspect of herbivory across vertebrates. Cell walls are typically broken down by translation of flattened teeth in the occlusal plane (i.e. grinding) as part of a complex, rhythmic chewing stroke. The grass carp, *Ctenopharyngodon idella*, is a voracious, invasive herbivorous fish that relies solely on its pharyngeal teeth, located in the back of the throat, for mechanical processing of plant material. Here, we describe the musculoskeletal anatomy of the pharyngeal jaws of grass carp and use XROMM to quantify chewing kinematics and muscle strain. The pharyngeal jaws are suspended in a sling of 11 muscles and maintain no bony articulation with any other skeletal elements in the head. The jaws bear long, serrated teeth that are worn during use into flattened tooth cusps. Our kinematic data show that this wear is the result of the teeth being elevated into occlusion against the basioccipital process and keratinous chewing pad, not tooth-on-tooth occlusion. Pharyngeal jaw elevation results from large strains in the jaw elevator muscle, the levator arcus branchialis V, to drive a pulley-like mechanism that rotates the jaws about a pivot point at the symphysis between the left and right pharyngeal jaws. These complex, rhythmic jaw rotations translate the teeth laterally across the chewing surface throughout the occlusion phase. The grass carp chewing system is strikingly similar in gross morphology and masticatory function to herbivorous chewing strategies in other vertebrates.

KEY WORDS: XROMM, Jaw, Biomechanics, Cyprinidae, Pharyngeal, Feeding

INTRODUCTION

Herbivory is a mechanically and chemically onerous trophic specialization, primarily because of the cellulose-rich walls that protect plant cells. Jawed vertebrates cannot produce enzymes that break down cellulose, so many herbivores harbor gut microbes that produce the appropriate enzymes (Saha et al., 2006; Stayton, 2006; Fritz et al., 2010). Even aided by gut microbes, however, mechanical processing is key in raising the efficiency of herbivory (Reilly et al., 2001; Fritz et al., 2009; Schwarm et al., 2009).

Department of Ecology and Evolutionary Biology, Brown University, Providence, RI 02912, USA.
*These authors contributed equally to this work

‡Author for correspondence at present address: University of Washington, Friday Harbor Laboratories, 620 University Road, Friday Harbor, WA 98250, USA (gidmark@uw.edu)

Received 26 August 2013; Accepted 22 February 2014

Mechanical processing in herbivores is often accomplished by chewing with a pattern of repeated, rhythmic biting movements (e.g. Schwenk and Rubega, 2005; Gintof et al., 2010). In evolutionary shifts to herbivory, chewing cycles increase in complexity of the rotational pattern of the jaw, which can increase the translation of one chewing surface relative to the other in the occlusal plane (Reilly et al., 2001). By translating one chewing surface relative to another, shearing forces are imparted onto the food, thereby rupturing plant cell walls (Rensberger, 1986). This shift toward increased translation has occurred several times within both Mammalia and Squamata (Reilly et al., 2001).

Grass carp, *Ctenopharyngodon idella* (Valenciennes 1844), is an herbivorous fish species native to Eastern Asia. Outside Asia, grass carp have been widely stocked for the control of aquatic vegetation, as adults grow up to a meter in length and consume up to 40% of their body mass in vegetation per day (USFWS, 2004). These freshwater ‘pond cows’ are nearly exclusively herbivorous as adults (Cudmore and Mandrak, 2004).

The oral jaws of the grass carp, like nearly all members of the family Cyprinidae, are edentulous and their only means of mechanical food processing is via a derived gill arch morphology, where the posterior-most gill arch processes food in the pharynx (Fig. 1). Pharyngeal teeth develop in the pharyngeal dermis and subsequently ankylose onto a hypertrophied fifth ceratobranchial, the sole remaining element of the fifth gill arch. The ceratobranchials are suspended in a muscular sling, and the pharyngeal teeth form the ventral occlusal surface. The dorsal occlusal surface is formed by the basioccipital process, a bony extension of the occipital bone of the neurocranium (Sibbing, 1982). Though chewing has been reported in grass carp (Vincent and Sibbing, 1992), the extent to which these herbivores conform to classical mammalian herbivory paradigms – multiple successive rhythmic chewing strokes, complex rotation of the jaws, lateral translation of flattened teeth – has not been investigated previously. Therefore, we hypothesize that during feeding, carp use rhythmic chewing strokes organized into successive trains, complex jaw rotations and lateral translations of flattened teeth.

In this study we use X-ray reconstruction of moving morphology (XROMM), a three-dimensional (3D) skeletal imaging technique, to explore movements of the grass carp pharyngeal chewing system *in vivo*. We quantify six-degree-of-freedom movements of the jaw as a whole, track the movement of specific tooth cusps, and measure muscle length dynamics throughout the chewing stroke. Using these data, we aim to: (1) demonstrate that accepted functional correlations between herbivore anatomy and mastication in amniotes are also present in a ray-finned fish; (2) provide one of the first 3D, six-degree-of-freedom analyses of gnathostome jaw movements during chewing; and (3) describe a new gnathostome chewing mechanism and its implications for food processing in cyprinid fishes.

The Journal of Experimental Biology (2014) doi:10.1242/jeb.096248

List of abbreviations

3D	three-dimensional
ACS	anatomical coordinate system
CPE	m. cleithropharyngeus externus
CPI	m. cleithropharyngeus internus
DLT	direct linear translation
JCS	joint coordinate system
TVV	m. transversus ventralis
XROMM	X-ray reconstruction of moving morphology

RESULTS

Anatomy

As in other cyprinids (Sibbing, 1982), the ceratobranchials are the only remaining element of the fifth pharyngeal arch, and teeth protrude medially from each arch (Fig. 1). No bony connections hold the grass carp pharyngeal jaws in place. The pharyngeal jaws are suspended in a sling of 11 muscles, five paired and one unpaired, and sit posterior to the gills and antero-medial to the pectoral girdle. The left and right jaws are joined at a flexible anteroventral symphysis and a single thin muscle (Fig. 1C). Our investigation focused on the largest pharyngeal jaw muscles, the m. levator arcus branchialis V (hereafter 'levator'), a hypertrophied branchial levator, and the m. retractor os pharyngeus (hereafter 'retractor'), derived from the m. sphincter oesophagi (Sibbing, 1982). Both of these muscles are laterally paired. The retractor has two parts, m. retractor os pharyngeus superioris and m. retractor os pharyngeus inferioris (Fig. 1A,C). They have contiguous origins and insertions and the same line of action, so for simplicity we combine them here as the retractor.

In grass carp, the levator and retractor make up nearly 80% of the pharyngeal jaw muscle mass, with the levator alone making up 66%. In addition, these are the only two muscles that have an appropriate line of action to play a role in occlusion. The levator has a broad and complex origin in the large subtemporal fossa (Fig. 1B,D), which in grass carp takes up most of the caudal third of the neurocranium. It inserts broadly along the curved dorsal ramus of the pharyngeal jaw (Fig. 1A). The retractor has a somewhat simpler origin along the posterior margin of the basioccipital process and inserts along the lateral, posterior aspect of the pharyngeal jaw (Fig. 1B–D).

Three other muscles are present in the pharyngeal jaw system of grass carp: the m. cleithropharyngeus externus (CPE), the m. cleithropharyngeus internus (CPI) and the m. transversus ventralis (TVV). The CPE and CPI originate on the pectoral girdle and insert on the ventral margin of the pharyngeal jaw, thus pulling the pharyngeal jaw anteroventrally and posteroventrally, respectively (Fig. 1A). While the CPE and the CPI are both laterally paired, the TVV is unpaired, running between the left and right jaws (Fig. 1C).

Pharyngeal teeth develop in the pharyngeal dermis and gradually ankylose with the fifth ceratobranchial. Serial waves of enamel and dentine form the tooth cusp (Fig. 2). After ankylosis, the teeth are functional and these serial waves are worn down to a flat tooth cusp (Fig. 2B,C versus Fig. 2E,F). This characteristic tooth-wear pattern is not observed on the sides of tooth cusps (where they pass by teeth from the opposing jaw), only on the area of the tooth that is oriented towards the basioccipital pad.

The left and right pharyngeal teeth interdigitate, but do not occlude with one another (Fig. 3). Instead, both the left and right jaws occlude against a keratinous pad that is firmly attached to a robust, flared basioccipital process on the base of the skull (Figs 1, 3). Laterally oriented grooves on the ventral base of the basioccipital pad are created by the consistent, precise occlusion of the teeth on the chewing pad (Figs 1, 3).

Muscle dynamics

As gape decreased and the teeth were brought toward occlusion with the basioccipital pad (Fig. 3), both the levator and the retractor shortened (Fig. 4, Fig. 5A). The levator muscle then continued to shorten throughout the occlusal phase of the chewing cycle, while the teeth were drawn laterally across the basioccipital pad. In contrast, the retractor muscle typically lengthened during occlusion

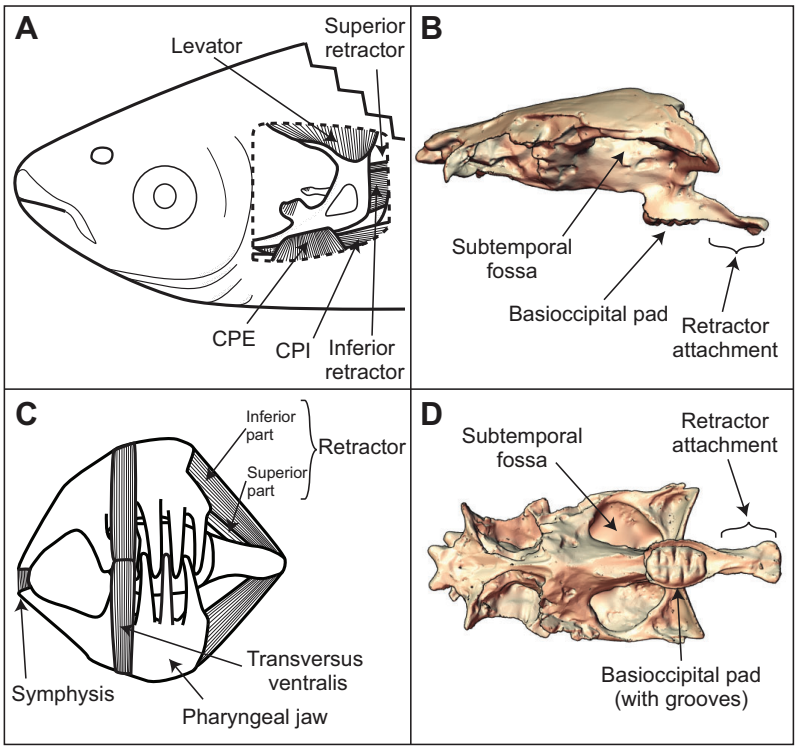

Fig. 1. Pharyngeal jaws of grass carp (*Ctenopharyngodon idella*). Anterior is to the left in all images. (A) Lateral view with operculum and gills removed to show pharyngeal jaws and musculature. (B) Lateral rendering from a laser scan of the neurocranium showing the basioccipital process with occlusal pad attached. (C) Ventral view of the jaws (the fifth ceratobranchials on left and right), basioccipital process (visible between the pharyngeal teeth) and a few muscles. (D) Ventral rendering of the neurocranium. Note the grooves on the basioccipital pad from chewing wear. Also note the broad insertion site of the levator muscle in the subtemporal fossa. CPE, m. cleithropharyngeus externus; CPI, m. cleithropharyngeus internus; levator, m. levator arcus branchialis V; retractor, m. retractor os pharyngii.

The Journal of Experimental Biology (2014) doi:10.1242/jeb.096248

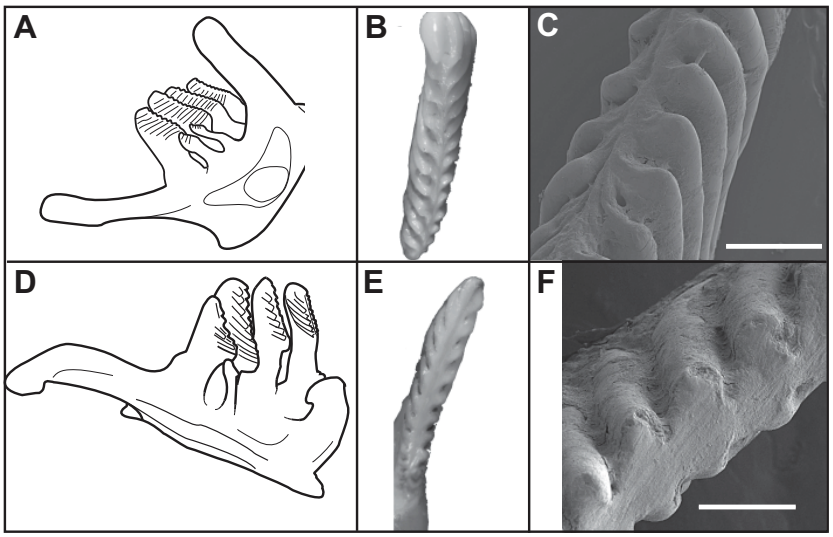

Fig. 2. Pharyngeal teeth of grass carp (*C. idella*). (A) Oblique lateral view of left pharyngeal jaw. Anterior is to the left. (B) Occlusal view of a developing (unworn) tooth; note smooth surface entirely covered by enamel. (C) Scanning electron micrograph (SEM) of the occlusal surface of a developing tooth. (D) Dorsal (occlusal) view of left pharyngeal jaw. Anterior is to the left. (E) Occlusal view of a functional (worn) tooth; note the flat occlusal surface with sharper edges. (F) SEM of a worn tooth; note the flattened chewing surface.

(Fig. 4, Fig. 5A). Therefore, peak shortening of the retractor occurred close to the onset of occlusion, whereas peak shortening of the levator occurred at the end of the occlusion phase. Despite differences in timing, both muscles undergo ~10% strain throughout the chewing cycle.

Jaw kinematics

At the start of a chewing cycle, the pharyngeal jaws are medially rotated (positive rotation about the *Z*-axis, relative to neurocranium) and elevated (negative rotation about *X*) so that the teeth come into contact with the basioccipital chewing pad (Fig. 3, Fig. 5B; supplementary material Movie 1). The power stroke involves lateral rotation (negative rotation about *Z*) and roll (positive rotation about *Y*) with the teeth remaining elevated against the chewing pad. Then the jaws are depressed in preparation for the next chewing cycle via positive rotation about *X* and *Z* and negative rotation about *Y* (Fig. 5B). We attempted multiple other positions of the joint coordinate system (JCS) aside from the symphysis between jaws in an effort to reduce the dimensionality of jaw movements, but we were unsuccessful. No matter where we placed the JCS, all three axes showed large rotations. The symphysis placement resulted in the smallest translations in all three axes, so we relied exclusively on this placement.

Though the jaws cannot translate relative to one another, they can translate together relative to the skull. These translations are relatively small (typically less than 2 mm; Fig. 5C). The main two translations are a small dorsal translation (positive *Z*) and a slightly larger posterior translation (negative *Y*). Dorsal translation of the jaws parallels that of the teeth (only smaller in magnitude, see below).

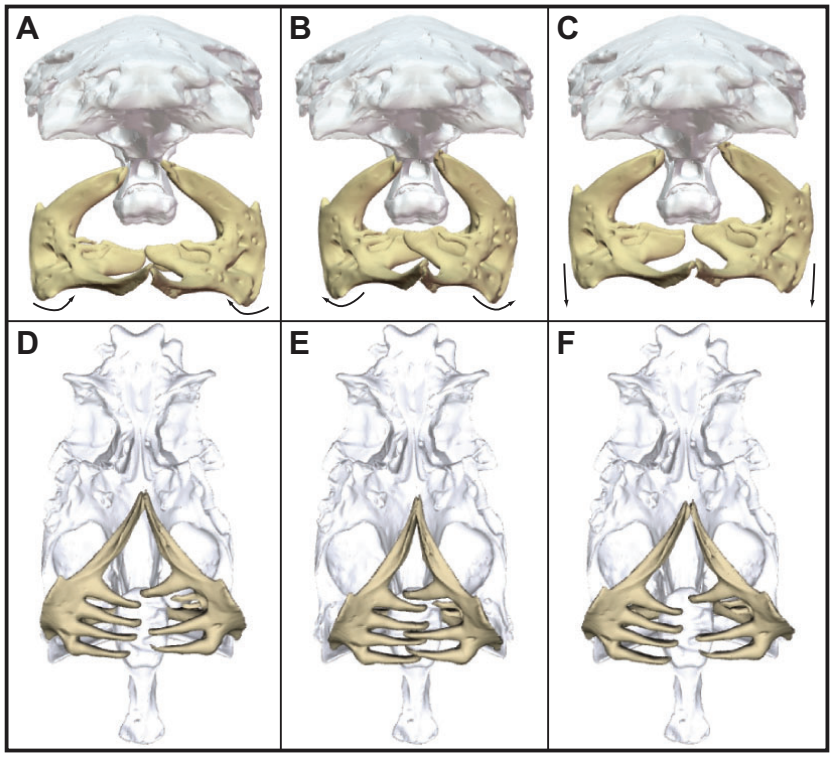

Fig. 3. XROMM animation of pharyngeal jaw kinematics. Frontal (A–C) and ventral (D–F) views of bones through one chewing cycle. In A and D, the jaws are 'open' and at their maximum distance from the basioccipital pad. In B and E, the jaws have rotated internally and have been elevated towards the occlusal surface. In C and F, external rotation has been completed and the teeth have been drawn across the occlusal for one chew stroke. The arrows show the direction of movement that will occur to move the jaws into the next position shown, with C referring back to A, as the motion is cyclical. This individual is missing one tooth on the left pharyngeal jaw.

The Journal of Experimental Biology (2014) doi:10.1242/jeb.096248

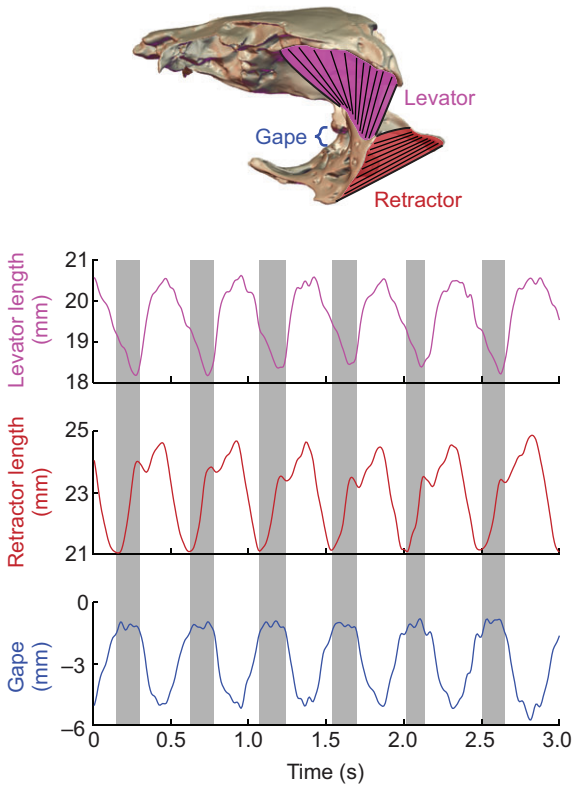

Fig. 4. Typical chewing sequence of six chewing cycles. As gape distance (blue) decreases (towards zero), the teeth are brought dorsally toward the chewing surface. We defined a threshold of <12.5% of maximum gape as the occlusion phase, shown in gray boxes here. Gape closure is accomplished by shortening of both the levator (pink) and the retractor (brown). At the onset of occlusion, the retractor begins to lengthen while the levator continues to shorten. Levator shortening continues throughout occlusion. Return of the jaws to the resting pose is associated with lengthening of both the retractor and levator.

Tooth kinematics

From a left tooth's perspective, elevation and medial movement (teeth from the left jaw actually cross the midline to begin occlusion on the right side of the basioccipital pad and vice versa) bring the tooth into occlusion. Negative *X*-axis rotation elevates the teeth into contact with the food bolus and basioccipital pad. Once the teeth touch the food, negative rotation about the *Z*-axis, combined with positive rotation about the *Y*-axis, results in predominantly lateral translations across the basioccipital pad in the occlusal plane (Fig. 5B,D). Slight posterior (negative *Y*) translation of the teeth is similar to translations of the jaws, but this translation is less than a third of the magnitude of the lateral translation. Dorsal translation (positive *Z*) remains constant through occlusion. These tooth motions result in wear of the functional teeth (Fig. 2).

Inter-individual and inter-cycle variability

One way to assess the variability of chewing cycle duration is to calculate the coefficient of variation (CV) (Gintof et al., 2010; Ross et al., 2007). Individuals 2, 3 and 4 each had a CV near or below 10% while individual 1 had a CV of 21%. All individuals produced trains of five to 25 consecutive chewing cycles, interrupted by pauses. We included all of the chewing cycles from all trains of chewing for each individual. A paired *t*-test showed that inclusion of the first and last chews from a train did not affect the overall CV (P=0.1035). Frequency of chewing was similar across the four individuals (1.85, 1.97, 2.39 and 2.14 Hz).

DISCUSSION

Grass carp show striking anatomical, kinematic and functional similarities to amniote herbivores. During the long occlusion phase, jaw adductor shortening results in lateral translation of the tooth cusps along the chewing surface (Figs 3, 5). At the level of the tooth, this chewing stroke approximates the grinding motion seen in amniote herbivores (Reilly et al., 2001). While the grinding motion of the tooth is similar to that observed in mammals, the chewing mechanism is completely different: in grass carp, a single muscle is primarily responsible for elevation (i.e. biting force), and the architecture of the hard anatomy (teeth and basioccipital pad) converts that bite force into lateral translation of the tooth.

Bite mechanics

Both the levator and retractor produce active tension during the occlusal phase, as demonstrated by recordings of their electrical activity (Sibbing, 1982). Active lengthening of the retractor suggests function as a stabilizing strut during the power stroke (Fig. 5A), bringing the jaws together and maintaining their positioning during the power stroke. In contrast, active shortening of the levator during the occlusal phase suggests that it is doing the positive work on the food bolus (Fig. 5A); therefore, we conclude that the levator is the primary muscle responsible for food breakdown.

Conversion of linear muscle strain into jaw rotation, translation and bite force would be easiest with a jaw joint to create a reaction force, as is the case in most oral jaws (e.g. Herring, 2003). However, in the grass carp pharyngeal jaw there is no such joint. We conclude that it is the tooth-on-pad occlusion that provides a bite-reaction force to resist the linear (dorsal) action of the levator. Thus, the lateral translation of the teeth is caused by force exerted in a direction that is nearly orthogonal to the resultant tooth translation. Importantly, we infer that this mechanism invokes an obligate coupling between bite force and grinding motion in the grass carp.

Rotational independence between left and right pharyngeal jaws allows the tooth cusps to pull in opposite (lateral) directions along the basioccipital pad when interdigitated, facilitating shredding of the plant material on the inter-tooth level, while on a tooth cusp level, the food can be sheared. This is corroborated by the finding of Vincent and Sibbing (Vincent and Sibbing, 1992) that fecal matter from grass carp shows both of these types of mechanical breakdown.

Convergent function in herbivorous chewing

Several aspects of the grass carp chewing mechanism are similar to those seen in other herbivorous vertebrates: long, continuous trains of rhythmic chews involving lateral translation of one flat chewing surface relative to another. This movement is best, and perhaps only, accomplished with complex, multi-dimensional rotations of the jaws. The above-mentioned attributes are all consistent between herbivorous fishes, herbivorous lizards and herbivorous mammals (Schwenk and Rubega, 2005). Reilly et al. (Reilly et al., 2001) describe how lizards, as a rule, use jaw motions that are less complex than those of mammals, but that even within lizards, herbivores tend to have a more complex chewing stroke than carnivores.

We found that chewing cycle duration was highly stereotyped (*sensu* Wainwright et al., 2008). Gintof et al. (Gintof et al., 2010) compared the CV of oral chewing cycle duration among mammals, lepidosaurs and basal teleosts. The CV of grass carp pharyngeal

The Journal of Experimental Biology (2014) doi:10.1242/jeb.096248

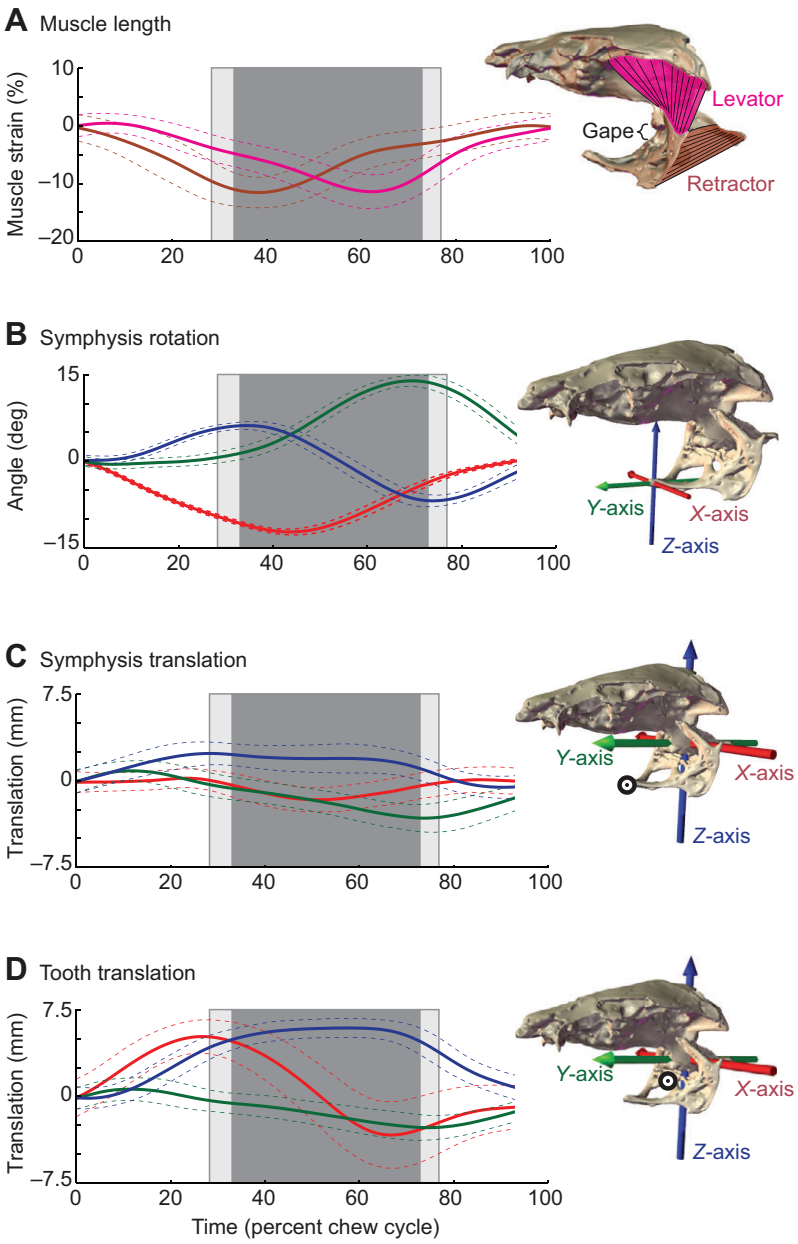

Fig. 5. Muscle dynamics and skeletal kinematics in the grass carp pharyngeal jaw. All panels contain summary data of the left jaw relative to the neurocranium, standardized by percentage of chewing cycle, for all individuals (*N*=4 individuals, *N*=202 total chewing cycles; 46–55 chewing cycles/individual). Data are means (solid lines), ± 1 s.d. (dotted lines). Dark gray boxes indicate times when the teeth are in occlusion with the chewing surface. Light gray bars represent ±1 s.d. in occlusion timing. (A) Muscle lengths for the retractor (brown) and levator (pink) muscles. (B) Rotations of the left pharyngeal jaw as measured by a joint coordinate system (JCS) placed at the symphysis between the left and right pharyngeal jaws. (C) Translations of the symphysis in neurocranium space from an anatomical coordinate system (ACS) at the back of the neurocranium. Tracking motion is based on a point (black/white bullseye) that is identical to the placement of the JCS. (D) Translations of a tooth cusp in neurocranium space relative to the reference posture at the beginning of the chewing sequence. In B–D, Red indicates *X*-axis movement, green indicates *Y*-axis movement, and blue indicates *Z*-axis movement (color scheme corresponds to JCS in Fig. 6C,D).

chewing, averaging 12%, falls among the least variable of the mammals and fishes, both of which ranged from 8% to 31%; lepidosaurs chew with much higher CV (mean of ca. 60%) than mammals and fishes (Gintof et al., 2010). This low level of variation appears to be accompanied by low flexibility (*sensu* Wainwright et al., 2008); a previous study found that grass carp did not modify their pharyngeal chewing rhythmicity in response to food material properties (Vincent and Sibbing, 1992).

The rhythmic grinding used by grass carp to break down their food results in substantial wearing of the tooth cusp. This wear exposes serial ridges of enamel between dentin, which we hypothesize act in the same way as the molars of many mammalian species (e.g. Rensberger, 1973). This self-sharpening mechanism results in a series of blades that are not only better suited for shearing plant material, but also concentrate the muscle stress on a smaller area, bringing the normalized bite force into a range that is more in accord with functional predictions (Vincent and Sibbing, 1992).

Divergent mechanisms in herbivorous chewing

Despite these functional similarities, the mechanism of food breakdown is different in grass carp as compared with mammals. In our hypothesized mechanism, a single jaw muscle is responsible for both bite force and lateral tooth translation movements, while other muscles serve mainly positioning and stabilizing functions. Mechanically, this contrasts with mammalian herbivores, where the muscle producing force (e.g. the masseter or the temporalis) might be different from the muscles that cause lateral translation of the teeth (e.g. the pterygoids) (Schwenk and Rubega, 2005). Therefore, in mammals, translation is at least partially decoupled from bite force. In our hypothesized mechanism for pharyngeal grinding in grass carp, it is in fact the bite force itself that causes lateral tooth translation, resulting in an obligate coupling between translation and bite force.

Concluding remarks

Our results demonstrate several hallmarks of amniote herbivory – rhythmic, complex jaw movements that act to translate flattened

The Journal of Experimental Biology (2014) doi:10.1242/jeb.096248

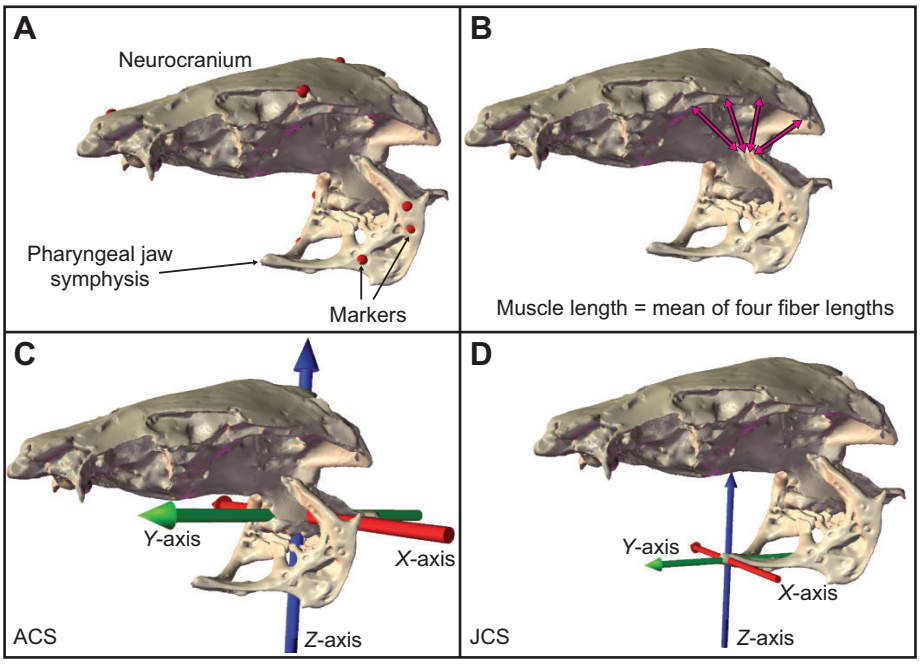

Fig. 6. Marker placement for XROMM animation and methods for data extraction. (A) Metal spheres were used as markers (red spheres) to align the laser-scanned bone model with kinematics from the X-ray videos. Three or more markers were placed on each bone of interest and care was taken to space the markers as widely as possible to increase overall bone tracking accuracy (Brainerd et al., 2010). (B) We took four measures of muscle length for the levator muscle and four for the retractor muscle. These represented the diversity of fiber orientations within each muscle. Muscle lengths reported here are means of the four fiber lengths at each time point. (C) We used an ACS for tracking translations of points on the jaw relative to the skull. We tracked the movement of a point on a tooth cusp to understand the relationship between whole-body movements of the jaw and translations of the tooth cusp. (D) We used a hierarchical axis setup, the JCS, to measure whole-bone rotations and translations. Axes indicate polarity of translations (along the axis, arrowhead indicates positive values) and rotations (about the axis, arrowhead indicates positive angle changes using the right-hand rule). Pharyngeal jaw motions at the symphysis were measured relative to the neurocranium.

tooth cusps in the occlusal plane – in a new taxon (teleost fish) and in an independent evolutionary acquisition of jaws. Despite morphological and functional similarities in these two herbivory systems, the mechanism of chewing is quite different: grass carp chew with their teeth against the base of the skull, not using tooth-on-tooth occlusion. This occlusion against the base of the skull replaces the jaw joint as a mechanism to convert linear action of the dorsally oriented levator muscle into lateral translation of the tooth against the chewing surface.

MATERIALS AND METHODS

Specimens

The 10 juvenile grass carp (all between 250 and 300 mm standard length, head lengths between 30 and 45 mm) examined in this study were obtained from farm-raised stock. In accordance with state regulations, all fish were verified as triploid and therefore sterile (Cassani and Caton, 1986). Four animals were used for *in vivo* data collection; the others were used for dissection and anatomical description. These four individuals were housed in custom-built, 150 l acrylic aquaria with a narrow, rectangular tunnel extension at one corner where the fish were trained to feed. These tunnels, 100 mm wide by 300 mm long, reduced the distance of water that X-rays would pass through while imaging feeding trials (Gidmark et al., 2012; Gidmark et al., 2013). Fish were maintained on pellet food and greenhouse-grown lawn grass (Scott's Turf Builder Sun and Shade Mix). All animal housing, maintenance and experimentation procedures were approved by Brown University's Institutional Animal Care and Use Committee.

Surgery and experimental protocols

In preparation for experiments, we surgically implanted radio-opaque tantalum spheres (Bal-Tec, Los Angeles, CA, USA), either 0.8 or 1.0 mm in diameter, into the neurocranium and pharyngeal jaws (Fig. 6A). Fish were anesthetized in tricaine methanesulfonate (Finquel MS-222, Argent Chemical Laboratories, Inc., Redmond, WA, USA) at an induction concentration of 0.1 g l^{-1} and then maintained at 0.075 g l^{-1} during surgery. Using a manual drill bit (McMaster-Carr, Robinson, NJ, USA), either 0.8 mm or 1.0 mm in diameter, we drilled holes into the bones of interest approximately equal in depth to the diameter of the marker and manually pressed the spheres into place. No incisions were necessary because the pharyngeal jaws were accessed through the opercular opening. We placed a minimum of three spheres in the neurocranium and three in each pharyngeal jaw. We took care to avoid co-linearity of spheres and to maximize distance between spheres to increase accuracy of movement reconstruction (Brainerd et al., 2010).

After marker implantation, the fish typically started eating again within 2 days. Once normal feeding resumed, the experimental aquarium was oriented with the tunnel in the field of view of a biplanar X-ray video system. Two C-arm fluoroscopes, OEC Model 9400 (Radiological Imaging Services, Hamburg, PA, USA), retrofitted with 30-cm diameter image intensifiers (Dunlee Inc., Aurora, IL, USA), were aligned such that the image intensifiers were approximately orthogonal to one another, and the two machines' fields of view overlapped. Feeding was imaged at 80–90 kVp and 20 mA. High-speed Photron 1024 PCI digital video cameras (Photron, Inc., San Diego, CA, USA) recorded videos from the fluoroscopes at 125 frames s^{-1}. We collected and analyzed a total of 202 chewing cycles from four fish feeding on grass. On all filming days, images of perforated metal grids and a 32-point calibration cube (described below) were also taken.

Undistortion, calibration and digitization

The resulting biplanar X-ray videos were processed using the XrayProject workflow to reconstruct 3D rigid body movements (Brainerd et al., 2010). We used XrayProject versions 2.2.0–2.2.3. This script package, updated

versions and related software are freely available at www.xromm.org, along with explanations and instructions. Using the XrayProject scripts with images of precision-punched steel sheets, we quantified distortion introduced by the X-ray image intensifiers. An undistortion transformation matrix was calculated in MATLAB (The MathWorks, Natick, MA, USA) to correct this distortion. Camera placement for each day of filming was calibrated using a 32-point calibration cube, constructed of acrylic sheets and 3 mm steel spheres, and direct linear transformation (DLT) techniques. To digitize marker positions of the animals over time, we tracked the two-dimensional positions of each bone marker in each camera view over the entire video sequence. The DLT calibration was used to calculate the 3D positions of each marker. We applied a low-pass Butterworth filter to the 3D coordinates with a cut-off frequency of 20 Hz (the fish chewed at ~2 Hz) to dampen marker-tracking error. Details of the XROMM technique and the associated MATLAB scripts are available at www.xromm.org (Brainerd et al., 2010). For each individual, we concatenated the *X*, *Y* and *Z* coordinates for each marker in each frame, across trials, for each individual. This gives a single time series of marker positions observed for each individual. Our four individuals had 5231, 6615, 3874 and 3664 frames of data, capturing 52, 55, 46 and 49 chew cycles, respectively. To measure precision in our analyses, we measured the standard deviation of distances between marker pairs implanted within the same bone. Across 12 marker pairs per individual and all video frames, the mean standard deviations for our four individuals were 0.064, 0.069, 0.061 and 0.057 mm, consistent with previous studies using this experimental setup (Brainerd et al., 2010; Dawson et al., 2011). The highest standard deviation was 0.079 mm between two neurocranium markers in individual 1 and the lowest was 0.046 mm between two pharyngeal jaw markers in individual 4.

Bone models and animation

Marker-based XROMM typically relies on a CT scan for alignment of digital bone models to marker centroids (Brainerd et al., 2010). Given the artifacts produced from tantalum beads in CT scans with small, thin fish bones, we opted for a laser-scan based workflow (Gidmark et al., 2012; Gidmark et al., 2013). After collecting muscle data, bones were cleaned by dissection and with dermestid beetles. To increase contrast for laser scanning, the bones were sprayed with Rust-O-Leum flat white spray paint (Painter's Touch Inc., Pleasant Prairie, WI, USA). We laser scanned the bones using a Microscan Tools scanner head with a Microscribe articulated arm (GoMeasure3D, Amherst, VA, USA) to create digital models of the bone surfaces. Models were processed in both Microscan Tools and Geomagic (Research Triangle Park, NC, USA) software. Because the keratinous basioccipital pad typically shrank during the drying process, we digitally substituted a cast of a scaled, hydrated pad for the purposes of visualization in the figures of this paper.

We took still X-ray images of each bone in front of the biplanar fluoroscopy system and undistorted/calibrated the images using the XrayProject scripts. These camera positions were imported into Autodesk Maya (Autodesk, San Rafael, CA, USA), along with the images of the bones and the laser-scanned bone models. We used Scientific Rotoscoping (Gatesy et al., 2010) to align the bone models to the still images of their radiographic shadows. Polygon spheres, 0.8 mm or 1.0 mm diameter, were then aligned to the markers also visible in the X-ray image to register marker placement within each bone. Once we had these relative marker positions and the 3D coordinates from digitizing, we calculated rigid body transformations, driving bone model movements based on marker positions using XrayProject and Autodesk Maya (Brainerd et al., 2010).

Data extraction from XROMM animations

We were interested in examining the length changes in two putative chewing muscles, the m. levator arcus branchialis V and the m. retractor os pharyngii (Fig. 1) during pharyngeal chewing. To measure muscle fiber length, we used the distance measure tool in Autodesk Maya, with one locator attached to a pharyngeal jaw and the other attached to the neurocranium (Fig. 6B). This measurement was taken across all frames of our animations. Both muscles have broad and irregular insertion sites; we took a mean of four representative attachment points, spanning the attachment areas, to approximate overall fiber strain of each muscle. The fiber insertion and origin sites were chosen based on several dissections of grass carp specimens including the experimental subjects. These sites were defined in Autodesk Maya with locators attached to the bone models prior to XROMM animation for each fish.

The XROMM workflow provides two major additional avenues to describe relative motion: anatomical coordinate systems (ACSs) and joint coordinate systems (JCSs). Because these are described in depth elsewhere (Brainerd et al., 2010; Dawson et al., 2011; Gidmark et al., 2012; Gidmark et al., 2013), we describe them briefly here. An ACS describes the motion of individual points relative to a reference bone in an anatomically oriented set of orthogonal axes (*X*, *Y*, *Z*). We placed an ACS on the basioccipital process and attached it to the skull (Fig. 6C). We oriented the *Z*-axis of the ACS dorsoventrally, and placed a virtual marker on the center of the occlusal surface of the anteriormost primary tooth. The *X*, *Y* and *Z* translations of this tooth relative to the neurocranium were exported in the ACS frame of reference, and we used the *Z* coordinate as our gape distance. Thus, regardless of anterior-posterior or medio-lateral translations of the jaw relative to the skull, we measure gape exclusively as the dorsoventral displacement of the teeth relative to the chewing surface. We defined the occlusion phase as times when gape was less than 12.5% of maximum gape for that individual. This range was a good selector for the inflection times of rotation about the *Z*-axis and gape measurement minima that indicated occlusion. We also tracked the *X*, *Y* and *Z* translations of the pharyngeal jaw symphysis in the same coordinate space. Only translations of the left jaw are reported here. Coordinates reported herein are relative to a reference posture, with the jaws flared laterally and depressed ventrally. This highly repeatable posture occurs at the beginning of the chewing stroke, making it a clear reference that can be confidently identified across individuals.

Relative whole-body movements of two bones can be tracked in a JCS. Similar to ACSs, JCSs are made up of *X*-, *Y*- and *Z*-axes. However, instead of all three axes being rigidly orthogonal as in an ACS, JCS axes are hierarchically related: the highest-order axis (in our case, the *Z*-axis) is rigidly attached to a proximal bone, and the lowest-order axis (in our case, the *X*-axis) is rigidly attached to a distal bone. The intermediate axis (our *y*-axis) is calculated as orthogonal to the other two axes. We used the neurocranium as the proximal bone and the left jaw as the distal bone. We placed the JCS at the anterior symphysis of the right and left pharyngeal jaws (Fig. 6D). The JCS allows measurement of the translations and rotations of the distal bone (pharyngeal jaw) relative to the proximal bone (neurocranium) about and along these axes (Brainerd et al., 2010; Grood and Suntay, 1983). These movements are calculated relative to the same zero position as mentioned for the ACS.

Data analysis

We wrote custom MATLAB scripts for data processing. Modifying a script written by C. A. V. Aguilera (extrema.m, www.mathworks.com), we defined the start and end of each chewing cycle from maximum opening to subsequent maximum opening and generated a matrix to indicate the start and end frame for each successive cycle. This start–end matrix was used to crop all five data streams: retractor muscle length, levator muscle length, tooth translation, jaw symphysis translation and jaw symphysis rotation. Each individual chew cycle was then spline-interpolated to 100 values so that between-cycle, between-individual and between-variable comparisons could be made.

Acknowledgements

We thank the Morphology group at Brown University, and particularly Nicolai Konow, Ariel Camp, Henry Astley and Thomas Roberts, for helpful discussions on the conceptual basis, experimental protocol and expression of this study. We thank Eric LoPresti for animal husbandry, Charles Vickers, Jr and Edward Mullen for advice on construction of the experimental apparatus, and Fred Jackson and Brian Leib at Brown's Environmental Plant Center for growing grass to feed our fish.

Competing interests

The authors declare no competing financial interests.

Author contributions

Conception of this study was by N.J.G. and E.L.B.; the study was designed by N.J.G., J.C.T. and E.L.B.; experiments were performed by N.J.G. and J.C.T.; data

were analyzed by N.J.G. and J.C.T.; results were interpreted by N.J.G., J.C.T. and E.L.B.; the manuscript was drafted by N.J.G. and J.C.T.; and edits to the manuscript were made by N.J.G., J.C.T. and E.L.B.

Funding

Generous funding support was provided by: the US National Science Foundation (0840950); the American Society of Ichthyology and Herpetology (Raney Fund); Sigma Xi GIAR; the W. M. Keck Foundation; and the Bushnell Graduate Education and Research Fund.

Supplementary material

Supplementary material available online at
http://jeb.biologists.org/lookup/suppl/doi:10.1242/jeb.096248/-/DC1

References

Brainerd, E. L., Baier, D. B., Gatesy, S. M., Hedrick, T. L., Metzger, K. A., Gilbert, S. L. and Crisco, J. J. (2010). X-ray reconstruction of moving morphology (XROMM): precision, accuracy and applications in comparative biomechanics research. *J. Exp. Zool. A* **313**, 262-279.

Cassani, J. R. and Caton, W. E. (1986). Growth comparisons of diploid and triploid grass carp under varying conditions. *Prog. Fish-Cult.* **48**, 184-187.

Cudmore, B. and Mandrak, N. E. (2004). Biological synopsis of grass carp (*Ctenopharyngodon idella*). In *Canadian Manuscript Report of Fisheries and Aquatic Sciences 2705*. Burlington, ON: Fisheries and Oceans Canada, Great Lakes Laboratory for Fisheries and Aquatic Sciences.

Dawson, M. M., Metzger, K. A., Baier, D. B. and Brainerd, E. L. (2011). Kinematics of the quadrate bone during feeding in mallard ducks. *J. Exp. Biol.* **214**, 2036-2046.

Fritz, J., Hummel, J., Kienzle, E., Arnold, C., Nunn, C. L. and Clauss, M. (2009). Comparative chewing efficiency in mammalian herbivores. *Oikos* **118**, 1623-1632.

Fritz, J., Hummel, J., Kienzle, E., Streich, W. J. and Clauss, M. (2010). To chew or not to chew: fecal particle size in herbivorous reptiles and mammals. *J. Exp. Zool.* **313A**, 579-586.

Gatesy, S. M., Baier, D. B., Jenkins, F. A. and Dial, K. P. (2010). Scientific rotoscoping: a morphology-based method of 3-D motion analysis and visualization. *J. Exp. Zool.* **313**, 244-261.

Gidmark, N. J., Staab, K. L., Brainerd, E. L. and Hernandez, L. P. (2012). Flexibility in starting posture drives flexibility in kinematic behavior of the kinethmoid-mediated premaxillary protrusion mechanism in a cyprinid fish, *Cyprinus carpio*. *J. Exp. Biol.* **215**, 2262-2272.

Gidmark, N. J., Konow, N., LoPresti, E. and Brainerd, E. L. (2013). Bite force is limited by the force–length relationship of skeletal muscle in black carp, *Mylopharyngodon piceus*. *Biol. Lett.* **9**, 20121181.

Gintof, C., Konow, N., Ross, C. F. and Sanford, C. P. J. (2010). Rhythmic chewing with oral jaws in teleost fishes: a comparison with amniotes. *J. Exp. Biol.* **213**, 1868-1875.

Grood, E. S. and Suntay, W. J. (1983). A joint coordinate system for the clinical description of three-dimensional motions: application to the knee. *J. Biomech. Eng.* **105**, 136-144.

Herring, S. W. (2003). TMJ anatomy and animal models. *J. Musculoskelet. Neuronal Interact.* **3**, 391-394, discussion 406-407.

Reilly, S. M., McBrayer, L. D. and White, T. D. (2001). Prey processing in amniotes: biomechanical and behavioral patterns of food reduction. *Comp. Biochem. Physiol.* **128A**, 397-415.

Rensberger, J. M. (1973). An occlusion model for mastication and dental wear in herbivorous mammals. *J. Paleontol.* **47**, 515-527.

Rensberger, J. M. (1986). Early chewing mechanisms in mammalian herbivores. *Paleobiology* **12**, 474-494.

Ross, C. F., Eckhardt, A., Herrel, A., Hylander, W. L., Metzger, K. A., Schaerlaeken, V., Washington, R. L. and Williams, S. H. (2007). Modulation of intra-oral processing in mammals and lepidosaurs. *Integr. Comp. Biol.* **47**, 118-136.

Saha, S., Roy, R. N., Sen, S. K. and Ray, A. K. (2006). Characterization of cellulose-producing bacteria from the digestive tract of tilapia, *Roeochromis mossambica* (Peters) and grass carp, *Ctenopharyngodon idella* (Valenciennes). *Aquac. Res.* **37**, 380-388.

Schwarm, A., Ortmann, S., Wolf, C., Streich, W. J. and Clauss, M. (2009). More efficient mastication allows increasing intake without compromising digestibility or necessitating a larger gut: comparative feeding trials in banteng (*Bos javanicus*) and pygmy hippopotamus (*Hexaprotodon liberiensis*). *Comp. Biochem. Physiol.* **152A**, 504-512.

Schwenk, K. and Rubega, M. (2005). Diversity of vertebrate feeding systems. In *Physiological and Ecological Adaptations to Feeding in Vertebrates* (ed. J. M. Starck and T. Wang), pp. 1-41. Enfield, New Hampshire: Science Publishers.

Sibbing, F. A. (1982). Pharyngeal mastication and food transport in the carp (Cyprinus carpio L.): a cineradiographic and electromyographic study. *J. Morphol.* **172**, 223-258.

Stayton, C. T. (2006). Testing hypotheses of convergence with multivariate data: morphological and functional convergence among herbivorous lizards. *Evolution* **60**, 824-841.

USFWS (2004). *Asian Carp – Aquatic Invasive Species Issues, Program Accomplishments and Program Needs*. Washington, DC: US Fish and Wildlife Service.

Vincent, J. F. V. and Sibbing, F. A. (1992). How the grass carp (Ctenopharyngodon idella) chooses and chews its food; some clues. *J. Zool.* **226**, 435-444.

Wainwright, P. C., Mehta, R. S. and Higham, T. E. (2008). Stereotypy, flexibility and coordination: key concepts in behavioral functional morphology. *J. Exp. Biol.* **211**, 3523-3528.